

Study of Effect of Convergence Section Geometric on the Performance of a Sonic Nozzle

F. A. Kassem^{1†}, A. A. Zahran¹ and M. Adel²

¹ Volume and Fluid Flow Metrology Laboratory, Mass and Force Division, National Institute of Standards (NIS), Giza 12211, Egypt

² Mechanical Power Engineering Department, Faculty of Engineering, Zagazig University, Zagazig 44519, Egypt

†Corresponding Author Email: fatma.abdelmordy@nis.sci.eg

ABSTRACT

Critical flow Venturi nozzles (toroidal, cylindrical, convergent–divergent, or C–D) nozzles) have discharge coefficients predicted through numerical and experimental investigations. Unfortunately, the imprecision of the critical-flow Venturi nozzle design makes it impossible to study the influence of inlet curvature R_c on the discharge coefficient in the laminar boundary layer area. This study examines how the inlet curvature affects the discharge coefficient, or C_d , in the laminar boundary layer area of a critical-flow Venturi nozzle with a cylindrical throat and toroidal shape. The inlet curvature has a range from one throat diameter to three and a half throat diameters. This range of inlet curvatures was obtained by throat the inlet of a high-precision nozzle that was primarily compliant with ISO 9300. The C-D nozzle showed the impact of the convergence angle on the discharge coefficient. The results showed that the highest discharge coefficient occurs at $R_c = 2d_{th}$ for a throat diameter of 0.5588 mm, whereas for $d_{th} = 3.175$ mm, it occurs at $R_c = 2.5d_{th}$ for toroidal nozzle. For this C-D nozzle, the highest discharge coefficient was observed to occur at a curvature of angle of 10° . Moreover, C_d increases significantly with increase of inlet stagnation pressure but with a small throat diameter.

Article History

Received December 5, 2024

Revised February 2, 2025

Accepted February 12, 2025

Available online May 5, 2025

Keywords:

Toroidal sonic nozzle

Curvature radius

Stagnation pressure

Discharge coefficient

Convergent- divergent nozzle

1. INTRODUCTION

Due to its structural simplicity and high precision, the sonic nozzle (SN), which is considered the major meter in gas flow standard facilities, has been widely used for measuring the flow rate quantity value, especially in the natural gas industry. SN is a venture tube with a convergent-divergent longitudinal section, and the smallest cross section is called “throat.” When the backpressure ratio (ratio of outlet to inlet pressures) is less than a certain value (called the “Critical Back Pressure Ratio” the flow speed at the throat reaches the local speed of sound. As the pressure drop between the inlet and throat (or constriction) of the nozzle increased, the flow rate increased until the sonic velocity was attained at the throat. At this point, the nozzle is “choked”, and the flow rate increases with the upstream pressure increment (eq. (1)). When the flow is choked the flow becomes insensitive to the downstream conditions. Any further decrease in the back-pressure ratio will no longer affect the flow speed at the throat, and the ideal mass flow rate can be calculated based on thermal dynamics theory. However, the real mass flow rate q_{mr} is always slightly smaller than the ideal mass flow rate q_{mi} . In this case, the flow rate is then influenced

by the geometry of the nozzle, the properties of the gas, upstream pressure and temperature. In ideal conditions, the parameters C_d , γ , P_{cr} take the values 1, 1.4, and 0.528 respectively. Since the flow is viscous and non-one-dimensional, the ideal and the actual mass flow rates are not the same and the difference can be calculated by eqs. (2), and (3). This deviation is expressed by the so-called: “discharge coefficient” Hall (1962), Stratford (1964), Kliegel, and Levine (1969), Tang (1969), Ishibashi (1999).

$$q_{mr} = C_d C^* A_{th} P_o \frac{1}{\sqrt{R T_o}} \quad (1)$$

$$q_{mi} = C^* A_t P_o \frac{1}{\sqrt{R T_o}} \quad (2)$$

$$C_d = \frac{q_{mr}}{q_{mi}} \quad (3)$$

Since 2011, Li and Johnson (2011), Li et al. (2010) have used a bilateral comparison between NIM (National institute of metrology of China) and NIST (National Institute of Standard and technology) to examine the impact of throat diameter and curvature radius (R_c) on the flow characteristics of nozzles with nominal throat diameters of 10 mm and 20 mm. The discharge coefficient

of sonic nozzles was examined by [Ishibashi \(2015\)](#) in relation to the intake curvature, inlet diameter, and diffuser length. After examining nozzles with throat diameters of 13.4 mm and 18.9 mm, they discovered that there were no appreciable variations in $C_{d,exp}$ and $C_{d,th}$ for $R_c > 1.5d_{th}$ and inlet diameter larger than roughly $2.5d$. However, when the inlet curvature was smaller than approximately $1.5d$, the discharge coefficient could not be estimated quantitatively, matching the ISO 9300 discharge coefficient by correcting the nozzle throat diameter [Nakao et al. \(2021\)](#). A technique was suggested to adjust the throat diameter such that the experimentally-determined discharge coefficient agrees with the ISO 9300 discharge coefficient. Thus, it can be concluded that an inaccurate throat diameter is a contributing factor to the discharge coefficient scatter. In fact, the scatter of the discharge coefficient can be considerably decreased by accurately correcting the throat diameter [Ishibashi \(2018\)](#). Investigated the laminar- turbulent boundary layer (BL) transition in toroidal-typed nozzles using linear stability analysis. They demonstrated that although the BL remained steady, the nozzle throat region was likely to experience a brief increase in energy, manifested by streamwise streaks [Zebrowski et al. \(2022\)](#). Using (RANS) turbulence models, they also studied numerically the transitional range effects of the boundary layer for toroidal-shaped nozzles with varying nozzle throat diameters. Their findings are in good agreement with the established correlation curves for toroidal nozzles [Ishibashi \(2015\)](#). However, they noted a diameter dependence on the transition onset and predicted a transitional range at higher Reynolds numbers [Ünsal et al. \(2016\)](#), [Weiss et al. \(2024\)](#). The impact of the wall roughness on the BL transition in toroidal CFVNs was studied through numerical simulations utilizing the transitional-turbulence model. The discharge coefficient decreased more strongly at higher relative roughness values, and the transition occurred earlier (at lower R_e values) ([Wang et al., 2019](#)). In 2018, an investigation carried out into the mechanism influencing the throat diameter effects on the boundary layer flow characteristics of a sonic nozzle found that the throat diameter affected both C_d and R_e ([Li et al., 2018](#); [Cao et al., 2023](#)). Over the last two years, it has been discovered that the surface roughness has a greater influence on the turbulent boundary layer than on the laminar boundary layer. As a result, it has been suggested that dimensionless relative roughness should be considered instead of absolute roughness values ([Wang et al., 2014](#); [Ding et al., 2015](#); [Ding et al., 2016](#)). Carried out an investigation to assess the impact of throat shaping on the internal efficiency of the nozzles. They examined five non-symmetrical converging-diverging nozzles in the Langley 16-foot transonic tunnel stationary test facility and collected internal performance data at various nozzle pressure ratios, reaching a maximum of 9.0 by [Mason \(1980\)](#). Delved into the realm of sonic nozzles used in gas flow-rate assessments. They discovered that the critical pressure ratio (CPR) was significantly influenced by the Reynolds number rather than the area ratio, particularly in scenarios with low flow speeds. Moreover, they noticed that the discharge coefficients for sonic nozzles fluctuate based on the flow geometry and Reynolds number, as they

reported and showed an increase in the discharge coefficient (C_d) as the mass flow rate escalates ([Park et al., 2001](#); [Spotts et al., 2013](#)). Avoiding a normal shock is largely dependent on the effect of the divergence angle on the mass flow rate across the sonic nozzles. When the divergence angle decreased and the throat diameter increased, the normal shocks traveled toward the nozzle outlet ([Shaalan et al., 2018](#); [Kassem et al., 2023](#)).

The present study focuses on the effect of different inlet curvature radii on the discharge coefficient and velocity distributions of sonic nozzles. The discharge coefficient C_d and geometric dimensions (d_{th} and R_c) of two sonic nozzles with throat diameters of 0.5588 and 3.175 mm were investigated at the National Institute of Standards. Different inlet geometries (sharp-edged for the C-D sonic nozzle) and rounded for the toroidal and cylindrical nozzles) can significantly influence the flow behavior in the converging section. This can affect the construction of boundary layers, development of flow acceleration, location of the normal shock occurrence, and total pressure drop across the nozzle. In addition, the performance was improved by minimizing the pressure loss. By comparing the changed geometries, designs that minimize pressure losses, maximize flow proficiency, and improve accuracy can be developed. In applications where, accurate flow measurements are critical (e.g., calibration standards), optimizing the geometry can improve the accuracy and repeatability of the nozzle. The implication of this study is that sonic nozzles play a critical role as secondary standards for the calibration of fluid-flow instruments. To maintain the impartiality of these calibrations, ensuring the highest possible sonic nozzle accuracy is of maximal importance. Sonic nozzles are frequently used as links in the traceability chain of national standards to preserve the traceability of the measurements. The integrity of this chain depends on the precise sonic nozzles, which guarantee that the flow measurements made in various laboratories and enterprises are comparable and consistent. Consequently, it is necessary to increase their accuracy and consider all the factors that influence their performance.

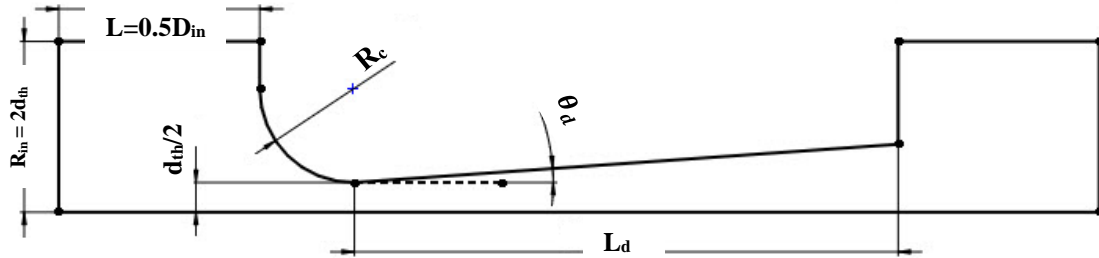
2. EXPERIMENTAL WORK

Three nozzles with different structures (toroidal, cylindrical, and C-D nozzles) were used in the simulation work. While toroidal nozzle was used in experimental work, the specification of test nozzle experimentally as shown in Table (1). Throat diameters of 0.5588 and 3.175 mm were investigating, as shown in Fig. (1), and (2). The steps of the present study are shown in the flowchart in Fig. (3). The nozzles were tested using a standard gas flow meter (piston prover) at a low flow rate of up to 30 l/min in NIS, Egypt, as shown in Fig. (4).

A device with an expanded uncertainty of 0.18% ($k = 2$) was used to calibrate the discharge coefficient of the sonic nozzle of throat diameter of 0.5588 mm at flow rates ranging from 4.13 to 12.12 l/min with stagnation pressures of 156.2 kPa, 450.09 kPa, respectively. The high flow rate was calibrated using a primary standard (Bell prover). This bell prover rig utilizes dry compressed air to

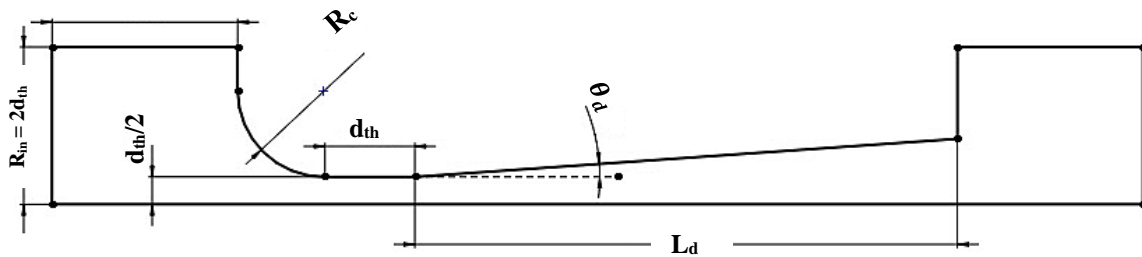
Table 1 Design and specification of test nozzles

Parameters	Values		
	Toroidal	Cylindrical	C-D
Nozzle type	Toroidal	Cylindrical	C-D
Throat diameter (d_{th})	0.5588, and 3.175 mm	0.5588, and 3.175 mm	0.5588, and 3.175 mm
Inlet curvature radii (R_c)	1, 1.5, 2, 2.5, 3, 3.5 d_{th}	1, 1.5, 2, 2.5, 3, 3.5 d_{th}	Convergent section at angles (4, 5, 6, 7, 8, 9, 10, 12, 14, 16, 18, 20, 22, 24, 26, 28, and 30°)
Divergence angle (θ_d)	4°	4°	4°
Divergence length (L_d)	7 d_{th}	7 d_{th}	7 d_{th}



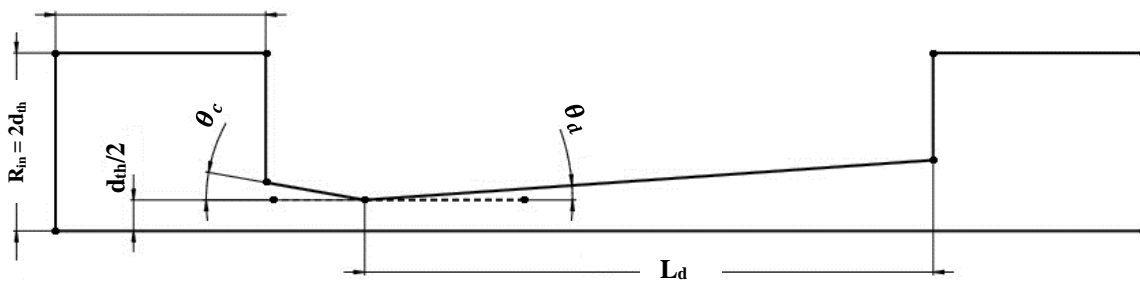
(a) Toroidal sonic nozzle

$L=0.5D_{in}$



(b) Cylindrical sonic nozzle

$L=0.5D_{in}$



(a) C-D sonic nozzle

Fig. 1 Schematic diagram for different sonic nozzle designs



(a) $d_{th} = 0.5588$ mm

(b) $d_{th} = 3.175$ mm

Fig. 2 Shape of toroidal sonic nozzle

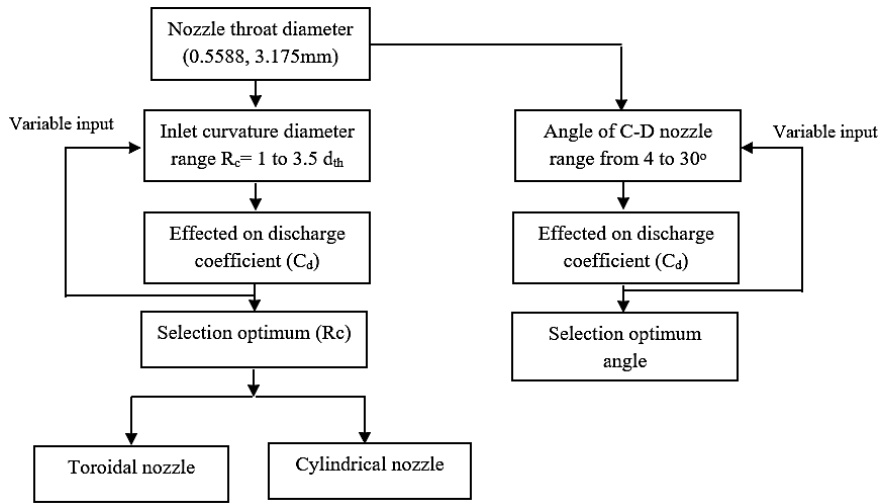
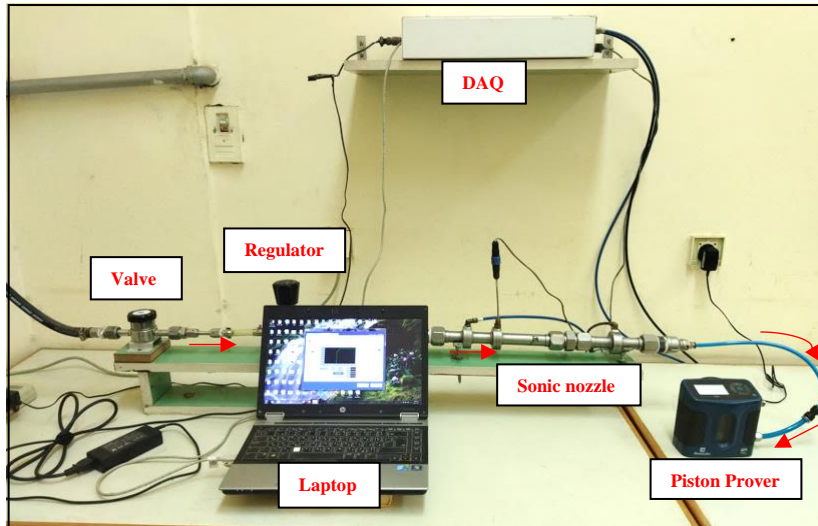
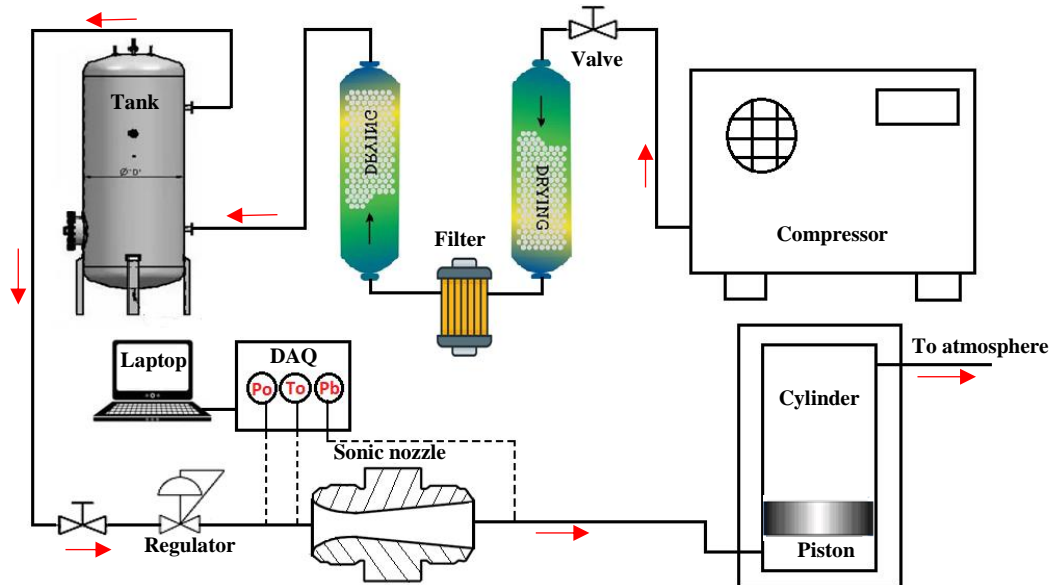


Fig. 3 Flow chart of present study



(a) Photo test rig of the sonic nozzle calibration



(b) Block diagram for the sonic nozzle calibration

Fig. 4 Test rig for calibration of sonic nozzle

calibrate the discharge coefficients of a sonic nozzle of throat diameter of 3.175 mm, covering a flow rate ranging from 129.75 to 405.50 l/min, and stagnation pressures ranging from 145.26 MPa to 450.09 MPa. The expanded uncertainty of the apparatus is 0.23% ($k = 2$). In addition, a fully-developed flow was created upstream of the nozzle to measure the repeatability, which was better than that of the simulation model.

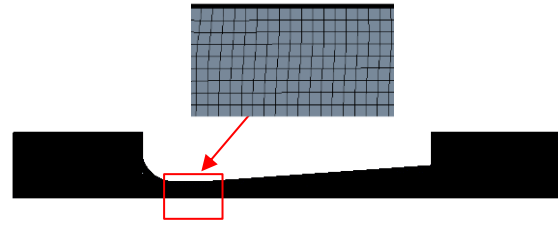
3. COMPUTATIONAL WORK

Since the nozzle longitudinal section was axisymmetric and using simple, toroidal, cylindrical, and C-D nozzle two-dimensional model, only half of the model longitudinal section was considered and the CFD mesh number thus decreased significantly. The number of grid elements is important in the computational analysis to ensure accuracy of the computed field variables. A fine grid requires excessive amounts of computational power and time to obtain a solution, whereas a coarse grid entails numerical errors and convergence problems. To test the independence of computational results on the grid number of cells, an unstructured mesh grid was generated in the specified computational domain using “CFD – Geometry” software. A variety of grid sizes were used, ranging from 4,791 to 17,722 nodes. The grid-sensitivity analysis was analyzed mainly to obtain grid-independent velocity along the wind tunnel at the axis of symmetry.

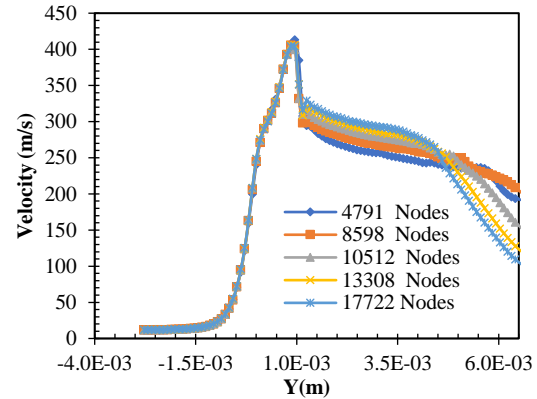
Figure (5) Shows the variation of the velocity distribution with computational grid size. The effect of grid size on the computed results diminishes for the grids of 13,308 nodes and more.

The three sonic nozzles had throat diameters of 0.5588 mm and 3.175 mm, an inlet curvature radius of $2d_{th}$, and a diffuser angle of 4° for the toroidal nozzle. The total number of mesh nodes was 13,308 with 12,923 elements. The governing eqs. (4) and (5) were solved using ANSYS Fluent software (R16). A density-based solver with an implicit formula suitable for high-speed compressible flows was adopted for the calculations, and was steady. Steady-state simulations are used in this study. Compared with transient simulations, steady-state simulations often use fewer input parameters and simpler mathematical models. This reduces the possibility of mistakes and streamlines the simulation setup. Furthermore, a steady-state simulation can supply the required data without simulating the full temporal development by concentrating on the end state, which is the primary interest in the system's final equilibrium state. The fluid was assumed to be an ideal gas, the operation pressure was zero, the inlet pressure ranged from 0.14 to 0.45 MPa, and the inlet stagnation temperature was fixed at 300 K. The back-pressure ratio was equal to or less than 0.69 to ensure that the throat flow could reach critical conditions to reliably compare the results with experimental data. The boundary conditions at the inlet and outlet of the sonic nozzle are presented in Table 2. The continuity and momentum conservation formulae are as follows [Fluent Inc \(2006\)](#).

$$\frac{\partial \rho}{\partial t} + \nabla \cdot (\rho U) = 0 \quad (4)$$



(a) Mesh shape for cylindrical nozzle



(b) Velocity distribution along axis of symmetry.

Fig. 5 Grid-independence solution for cylindrical nozzle of throat diameter 0.5588 mm

$$\frac{\partial}{\partial t} (\rho U) + \nabla \cdot (\rho U \cdot U) = -\nabla P + \nabla \cdot (\tau) + SM \quad (5)$$

For $k-\omega$ SST model, the turbulence kinetic energy k and the specific dissipation rate ω , which are modeled as:

$$\frac{\partial}{\partial t} (\rho k) + \frac{\partial}{\partial x_i} (\rho k u_i) = \frac{\partial}{\partial x_j} \left[\left(\mu + \frac{\mu_t}{\sigma_k} \right) \frac{\partial k}{\partial x_j} \right] + G_k - Y_k \quad (6)$$

$$\frac{\partial w}{\partial t} + \frac{\partial}{\partial x_i} (\rho w u_i) = \frac{\partial}{\partial x_j} \left[\left(\mu + \frac{\mu_t}{\sigma_w} \right) \frac{\partial w}{\partial x_j} \right] + G_w - Y_w + D_w \quad (7)$$

where, ρ and μ represent the gas density and kinetic viscosity. G_k and G_w are the generation of k and w due to mean velocity gradients. Y_k and Y_w represent the dissipations of k and w due to turbulence. D_w is a cross-diffusion term.

4. RESULTS AND DISCUSSION

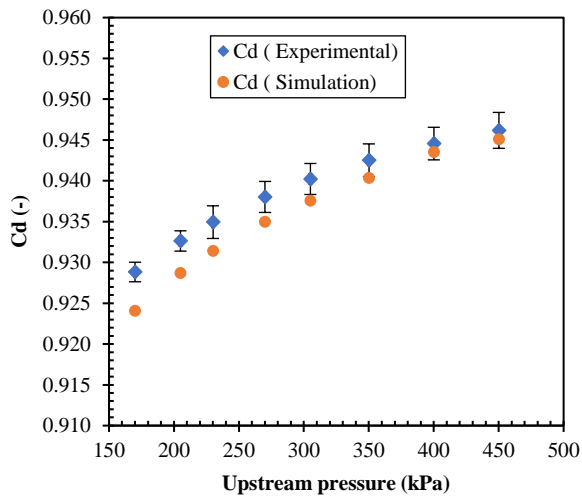
Validation between the experimental and numerical results for different throat diameters as shown in Fig. (6). The results indicate a maximum relative error of 0.41 %, which decreased with increase of upstream pressure to 0.13%. In addition, the discharge coefficient increases as throat diameter increases from 0.55588 to 3.175 mm with the same inlet operating condition (upstream pressure and temperature). Furthermore, owing to the substantial increase in the flow velocity, C_d increased as the inlet stagnation pressure increased. An increased velocity and less viscous effects may result in a thinner boundary layer. The uncertainty of experimental data between 0.1 to 0.23 %

Table 2 CFD model and boundary conditions

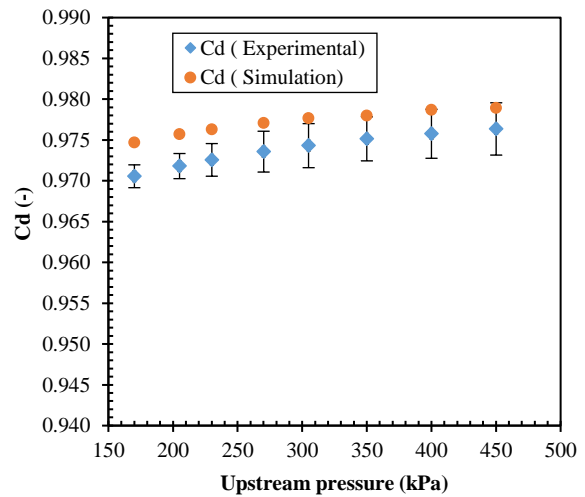
Condition	Type	Value
Time	Steady	
Turbulence model	RNG (k- ω)	
Inlet	Pressure inlet	Pressure inlet: 156410.3 Pa Temperature: 299.308 K
Outlet	Pressure outlet	Pressure: 101473.7 Pa Temperature: 299.308 K
Wall	Wall	Adiabatic
Solution method	Implicit	
Initialization methods	Hybrid	
Convergence residuals	10 ⁻⁶	
Maximum number of iterations	20,000	

Table (3) Uncertainty budget of measurement at $d_{th} = 0.5588$ mm and upstream pressure 450 kPa

Components	Distribution	Sensitivity coefficient	Divisor	Standard uncertainty (u)
Repeatability (%)	Normal	1	1	0.006
Reference flow meter (piston prover) (%)	Normal	1	1	0.11
Resolution (%)	Rectangular	1	$\sqrt{3}$	0.005
Drift (%)	Normal	1	1	0.03
Combined uncertainty (u_c) %	$\sqrt{(u_{Rep.})^2 + (u_{Ref.})^2 + (u_{Res.})^2 + (u_{drift})^2} = 0.11428$			
Expanded uncertainty (U) %	$k \times u_c = 0.228$			



(a) $d_{th} = 0.5588$ mm



(b) $d_{th} = 3.175$ mm

Fig. 6 Comparison between experimental and numerical work for different throat diameters

for throat diameter 0.5588 mm at confidence level ($k=95\%$). While at throat diameter 3.175mm the expanded uncertainty Ranging from 0.1 to 0.32%. Details of the evaluation of the expanded uncertainty of the sonic nozzle when calibrated using a piston prover are presented in Table 3. It should be noted that the experimental result was higher

than the simulation result, as shown in Fig. (6a). Uncontrolled climatic elements, such as humidity and temperature, blame this. Furthermore, there is always some degree of error in experimental measurements because they are not flawless. These mistakes may have resulted in an overestimation of the experimental findings. In addition,

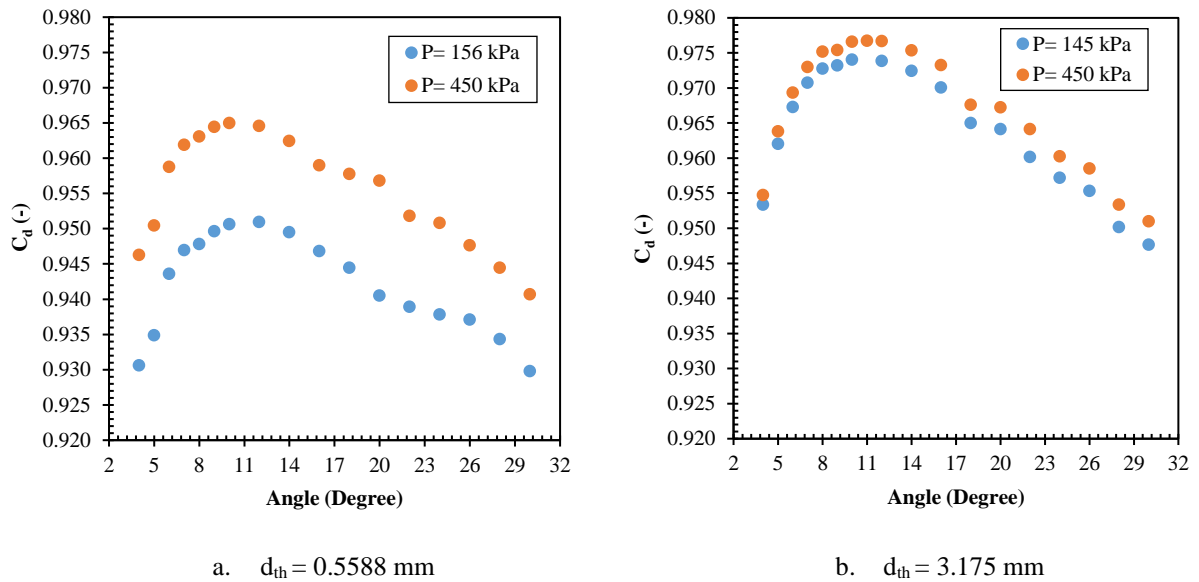


Fig. 7 Effects of convergence section angle on discharge coefficient for different stagnation pressures

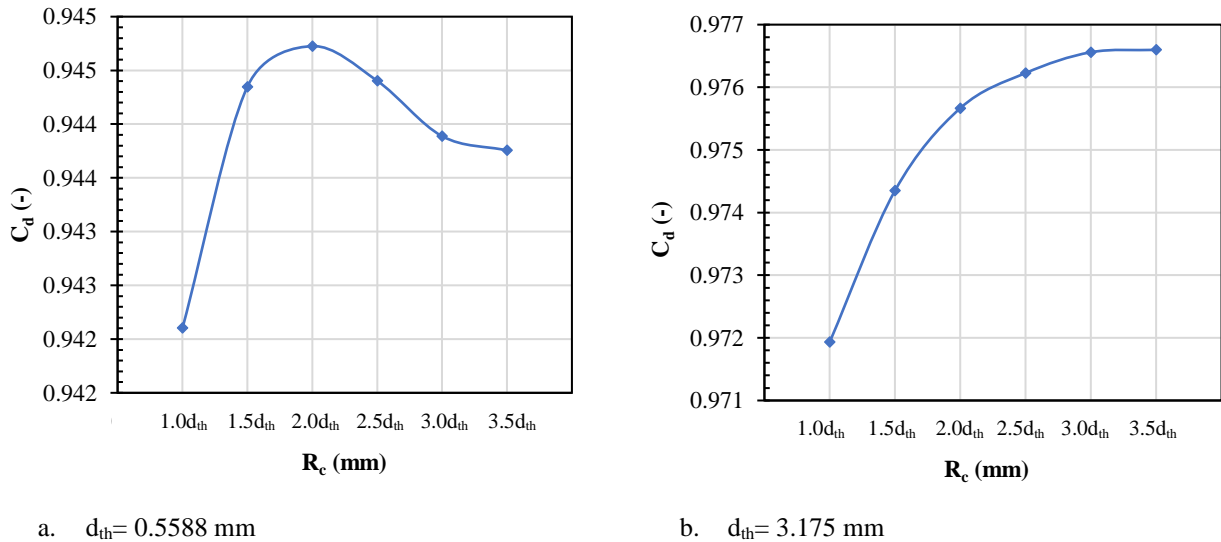


Fig. 8 Effects of inlet radius of curvature of toroidal nozzle for different throat diameters

errors due to human error occurred when the results were taken.

The effects of the converging part angles on C_d at different stagnation pressures are shown in Fig. (7). With the same upstream pressure of 156 kPa and an increase in the angle of convergence, C_d increased to reach an optimal angle of 10° . Subsequently, C_d began to decrease as the angle of convergence increased. Due to, when the convergence angle is too large (above 10°), shockwaves can form within the diverging section of the nozzle. These shock waves caused a sudden increase in the static pressure and a decrease in the flow velocity. This disrupts the smooth and supersonic expansion of the flow and reduces the overall nozzle efficiency. In addition, flow separation the presence of shock waves induces flow separation from the nozzle walls. This separation creates regions of recirculating flow and turbulence, which increase flow resistance. In addition, C_d increased significantly with an

increase in the upstream pressure with a small throat diameter due to the increase in the Reynolds number at the throat, which thins the boundary layer. For large throat diameters, C_d increases slightly.

The effects of the inlet radius of curvature of the toroidal nozzle at different throat diameters are shown in Fig. (8) For a throat diameter of 0.5588 mm, the discharge coefficient increases with an increase in the inlet radius of curvature until $R_c = 2d_{th}$ and then decreases gradually with R_c . This is because a sharper inlet curvature can result in an adverse pressure gradient near the nozzle entrance. In addition, the separated flow increased the resistance to flow and reduced the available flow area for the fluid to pass through. In addition, an adverse pressure gradient can cause the flow to separate from the nozzle wall. Consequently, the actual mass flow rate was reduced. For large throat diameters, the discharge coefficient increases slightly when R_c reaches a constant value at $3d_{th}$. This is due to the

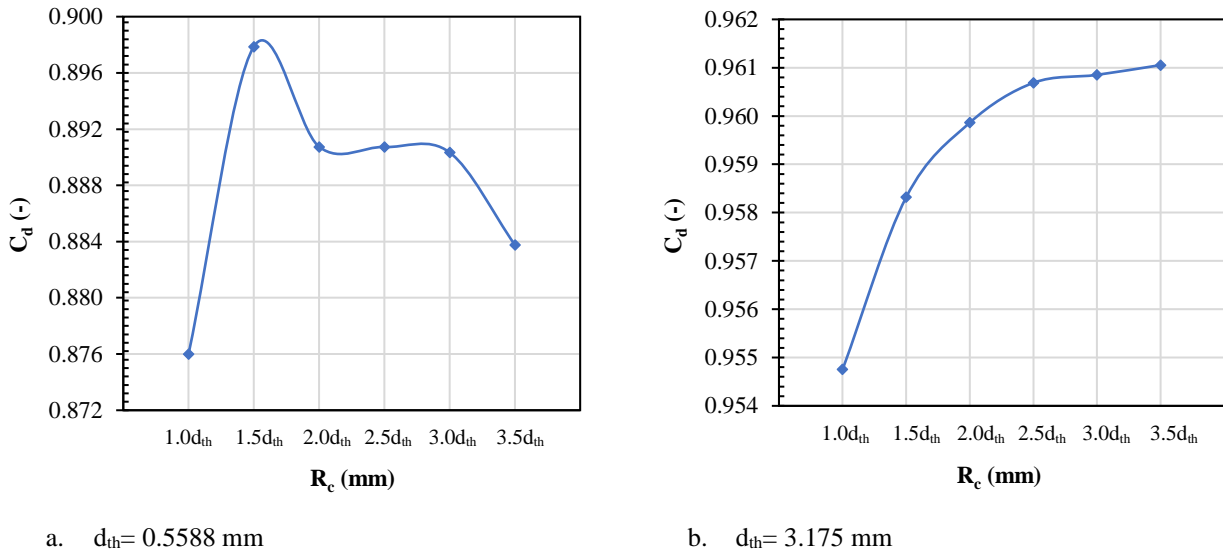


Fig. 9 Effects of radius of curvature of cylindrical nozzle inlet with different throat diameters

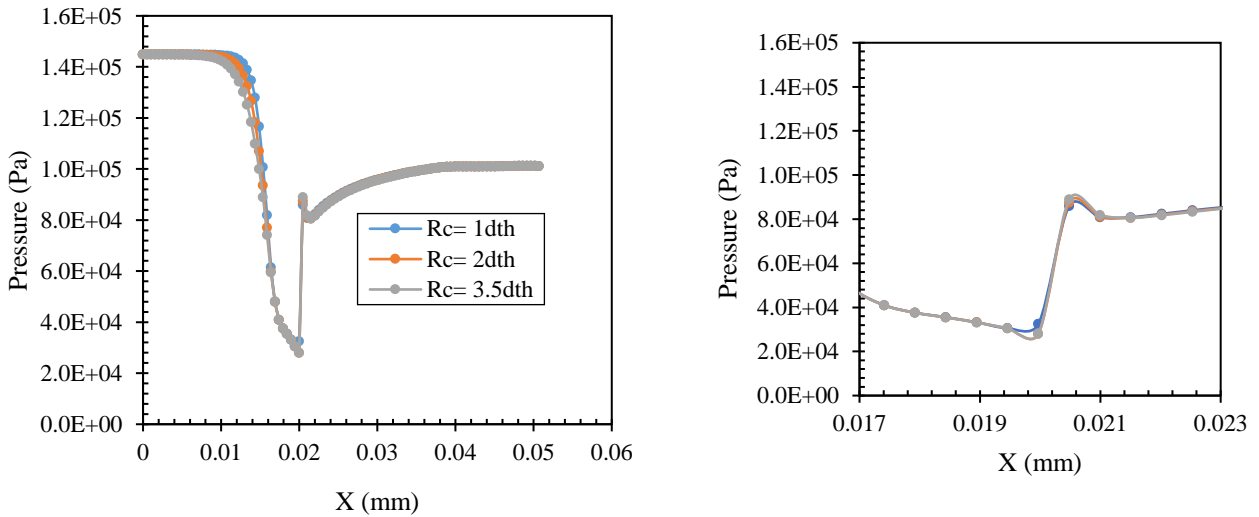


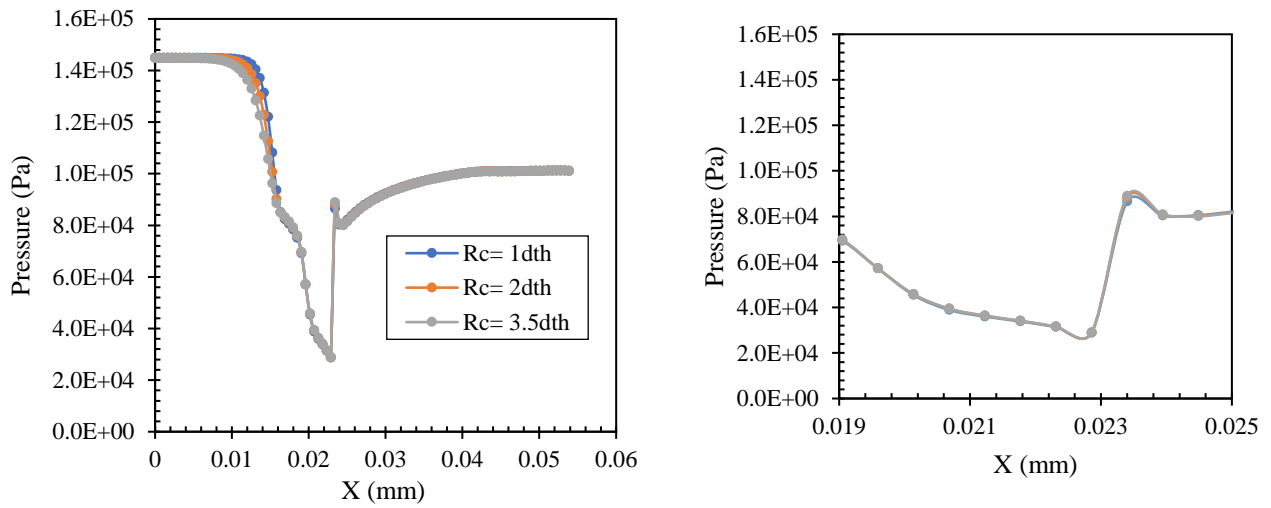
Fig. 10 Pressure distributions along toroidal sonic nozzle with different inlet curvature radius at $d_{th} = 3.175$ mm

reduction in the boundary layer growth, and smoother flow acceleration, ultimately resulting in an increase in the discharge coefficient. A cylindrical nozzle is similar to a toroidal nozzle, but flows separately early when the radius of curvature exceeds 1.5. This is due to the formation of a thicker boundary layer compared to that of the toroidal nozzle. For a small throat diameter of 0.5588 mm, the discharge coefficient increased gradually with an increase in the radius of curvature until $R_c = 1.5d_{th}$. Then, decreases once again as shown in Fig. (9.a). For a high throat diameter of 3.175 mm, the discharge coefficient increases gradually with R_c significantly from $R_c = 1$ to $2.5d_{th}$, then the discharge coefficient increase with R_c is very small or nearly constant when R_c is greater than $2.5d_{th}$ as shown in Fig. (9. b).

The pressure distributions along the toroidal and cylindrical sonic nozzles (axisymmetric) with different inlet curvature radii at a throat diameter of 3.175 mm are shown in Fig. (10, 11). When R_c increased, the flow velocity increased and the pressure decreased at the entrance

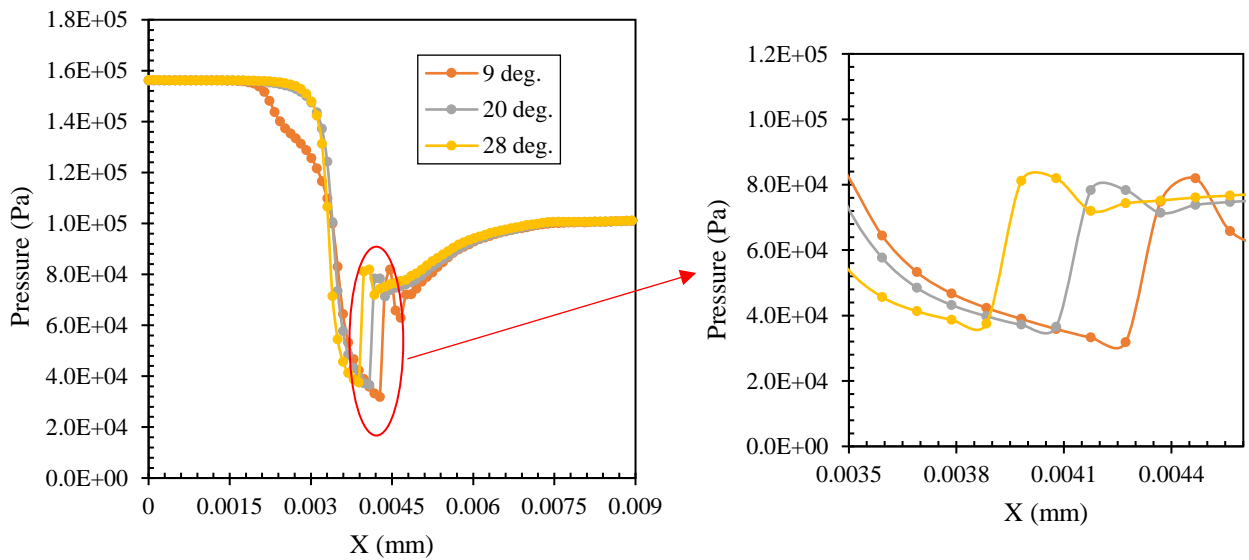
section; the effect of the inlet curvature radius was small at the inlet nozzle. The difference in R_c does not affect the pressure at the throat and divergence sections. This is due to the flow at the axisymmetric considered inviscid flow, and the flow is more aligned with the centerline from the start, reducing the influence of the inlet curvature on the pressure distribution along the centerline. For the C-D nozzle, the effect of the convergence angle on the location of the normal shock wave is significant, as shown in Fig. (11) for nozzle-throat diameters of 0.5588 and 3.175 mm, respectively. With a decrease in the convergence angle, the shockwave moves in the outlet direction. This is because the change in area was more gradual. This gentle change reduced the strength of the pressure waves generated due to the changing geometry. In addition, with a smaller convergence angle, the flow entering the diverging section is more uniform and exhibits fewer pressure disturbances.

Figure (13) depicts the velocity distributions across the throat diameter for convergence angles ranging from 8° to

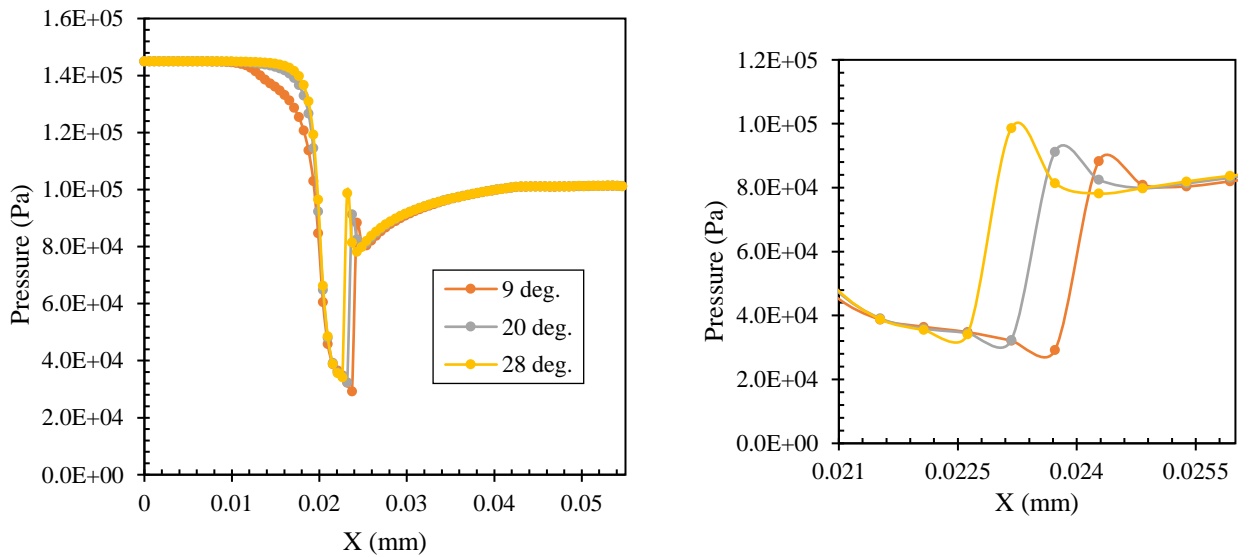


a) $d_{th} = 3.175$ mm

Fig. 11 Pressure distributions along cylindrical sonic nozzle with different inlet curvature radius at $d_{th} = 3.175$ mm

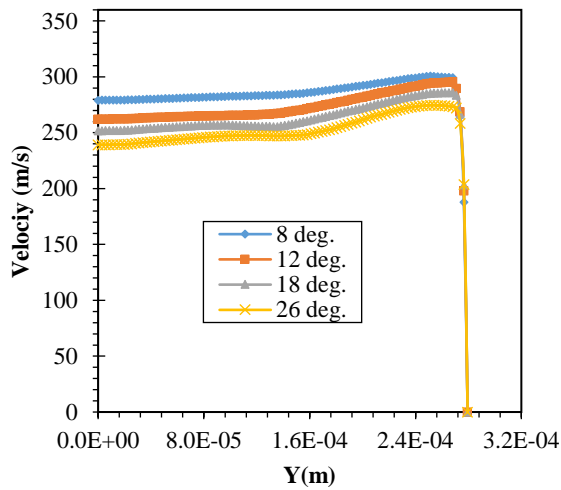


a) $d_{th} = 0.5588$ mm

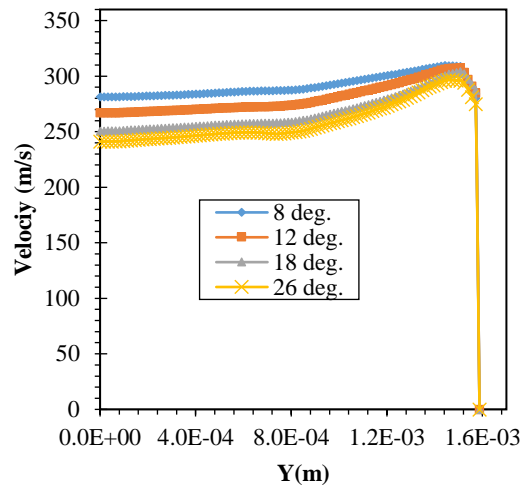


b) $d_{th} = 3.175$ mm

Fig. 12 Pressure distributions along C-D sonic nozzle with different inlet convergence angles and throat diameters

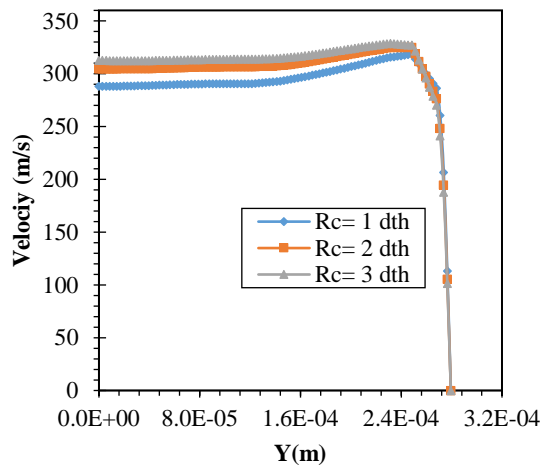


a. $d_{th} = 0.5588$ mm

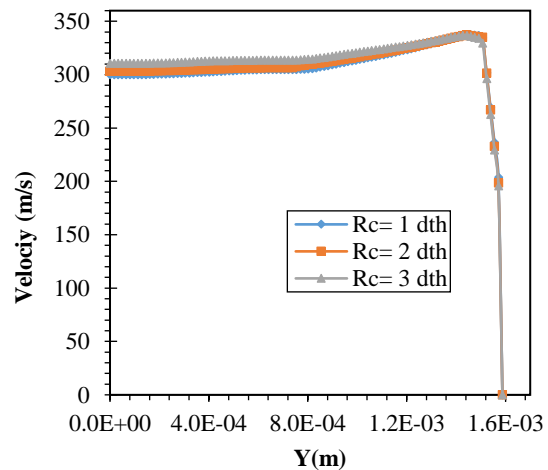


b. $d_{th} = 3.175$ mm

Fig. 13 Velocity distributions at throat diameter for different angles of convergence section for C-D nozzle



a. $d_{th} = 0.5588$ mm



b. $d_{th} = 3.175$ mm

Fig. 14 Velocity distributions across throat diameter for different radii of curvature inlet for toroidal nozzle

26°. These results show that the velocity increases with a decreasing convergence angle. This may be due to the resulting decrease in cross-sectional area. Moreover, the flow becomes more uniform with a convergence angle of 8° compared with higher angles, especially at an angle of 26°. As the throat diameter was increased to 3.175 mm, the boundary layer thickness decreased, and consequently, the velocity increased, as shown in Fig. (14). For a toroidal sonic nozzle, if the inlet curvature is large, the effects on the velocity distributions are significant. When R_c increased, the velocity increased for a small throat diameter, as shown in Fig. (14a). However, for a large throat diameter, the effect of R_c on the velocity distribution was not significant, as indicated in Fig. (14b). Because the flow reaches a fully developed flow. As the flow progresses downstream, it transitions from developing flow to fully developed flow. In a fully developed flow, the velocity profile remains constant and the effects of the inlet conditions diminish. This leads to the stabilization of the flow characteristics and, consequently, C_d .

This finding suggests that for larger throat diameters, the designer has more flexibility in choosing the inlet curvature without significantly affecting the velocity distribution at the throat. This can simplify the design process and reduce manufacturing costs. Also, may be less sensitive to small variations in inlet curvature during manufacturing, which can be beneficial for achieving consistent performance.

Figures (15) and (16) illustrate the velocity distributions across the throat diameter section for cylindrical nozzles with different R_c values. The throat was divided into three regions (starting, mid, and end regions). The velocity distributions appear to be affected by the change in R_c in the starting region, whereas in the mid- and end-regions, the distributions appear unaffected by a change in R_c . The velocity contours along the sonic nozzle longitudinal section with a throat diameter of 3.175 mm and inlet stagnation pressures of 145 kPa and 270 kPa are shown in Fig. (17). The initial stage of the inlet nozzle velocity flow is minimal. The Mach number (Ma) increases gradually, starting from the convergence section along the nozzle to

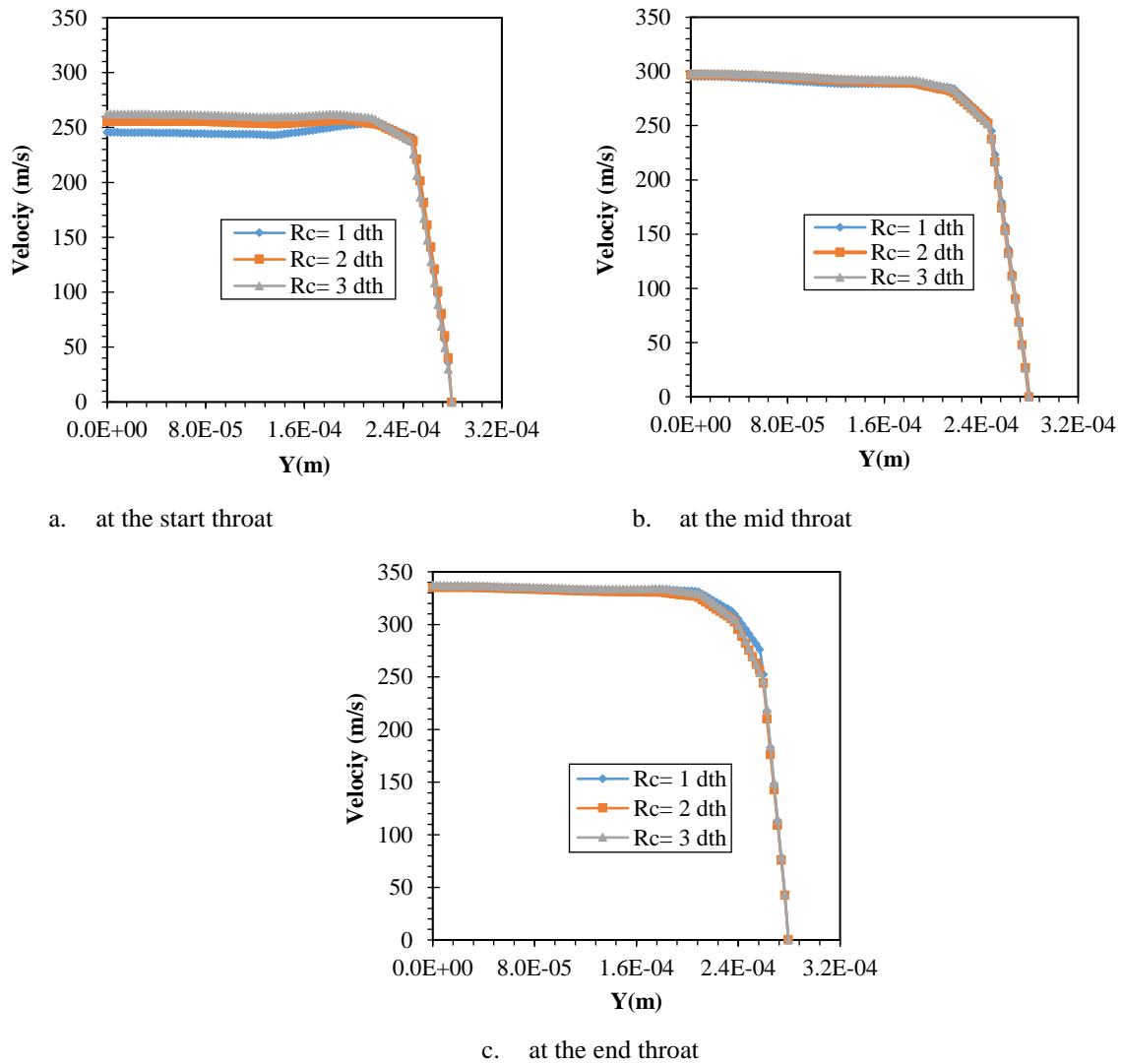


Fig. 15 Velocity distributions across throat diameter for different inlet radii of curvature of cylindrical nozzle and $d_{th} = 0.5588$ mm

reach the acoustic speed at the throat ($Ma = 1$). This process is referred to as flow-choking. Moreover, the Mach number increases along the sonic nozzle at a convergence angle of 8° compared to 26° , as shown in Fig. (17.a). Subsequently, it continued to increase until it reached a speed above the speed of sound, with a normal shock wave occurring in the divergent section (see Fig. (17.b)). The maximum Mach number reached speed is 2.3 (supersonic speed), followed by a decrease to subsonic speed after the normal shock. In addition, a vortex is formed close to the nozzle wall immediately after the shock due to the flow separation that occurs close to the nozzle outlet.

5. CONCLUSION

The aim of this study was to obtain the highest discharge coefficient to improve the measurement accuracy. The novelty of this study is the direct influence of the inlet curvature diameter on C_d , flow uniformity, and thickness of the boundary layer within the R_c range of 1 to $3.5 d_{th}$. Six values of the design R_c were used for the toroidal and

cylindrical nozzles. In addition, the effect of the convergence angle for the C-D nozzle in the range of $4-30^\circ$ was examined. The simulation was validated experimentally for a toroidal nozzle with $R_c = 2 d_{th}$ at the National Institute of Standards. It is generally concluded that R_c plays an important role in enhancing the C_d levels. From the obtained results, the following conclusions can be drawn:

1. The highest discharge coefficient was achieved at a convergence angle of 10° for throat diameters of 0.5588 mm and 3.175 -mm throat diameters.
2. For small throat diameters, the discharge coefficient increases significantly with the inlet stagnation pressure. Due to the flow velocity increased significantly. This can lead to a thinner boundary layer due to increased momentum and reduced viscous effects.
3. For the toroidal nozzle, the highest discharge coefficient occurs at $R_c = 2d_{th}$ with a throat diameter of 0.5588 mm, whereas for $d_{th} = 3.175$ mm, $R_c = 3d_{th}$.

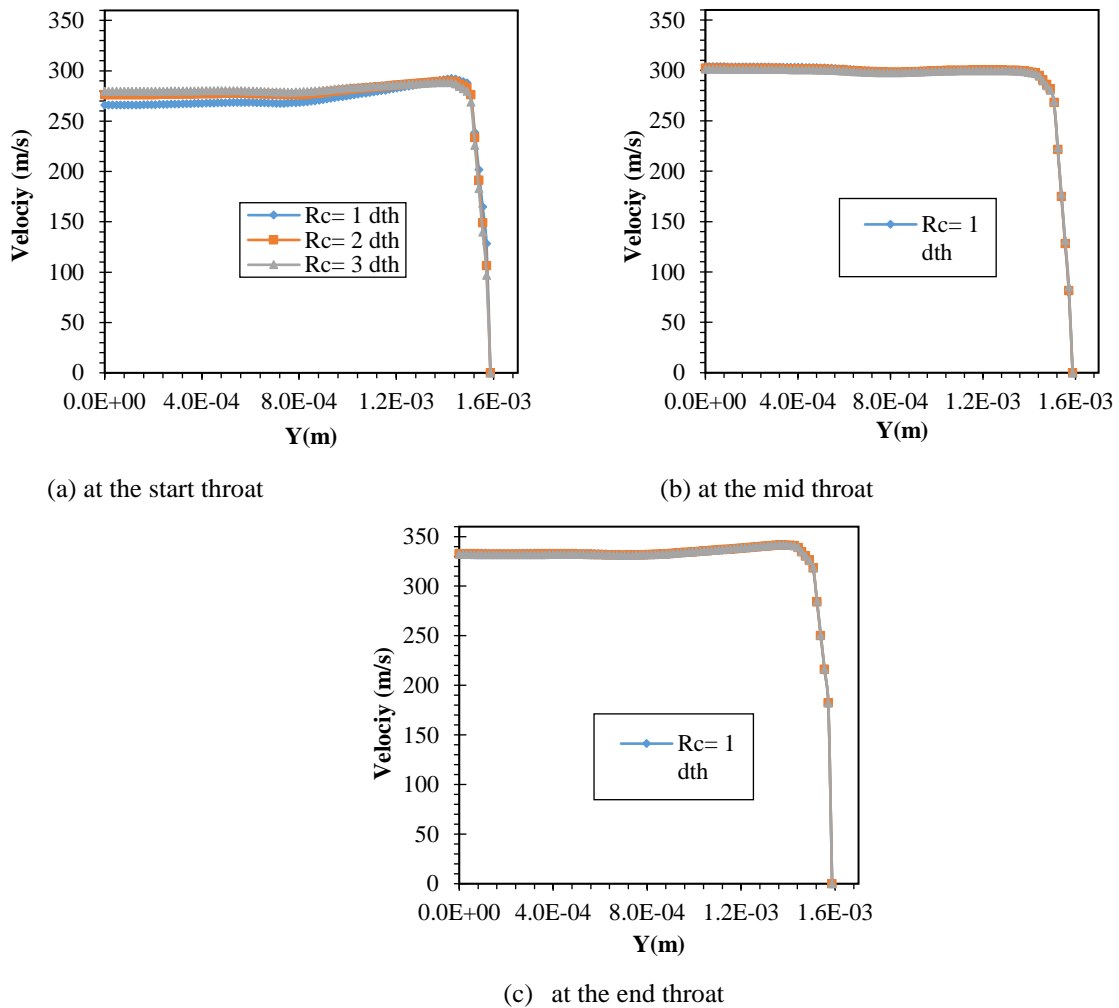


Fig. 16 Velocity distributions across throat diameter for different inlet radii of curvature of cylindrical nozzle with $d_{th} = 3.175$ mm

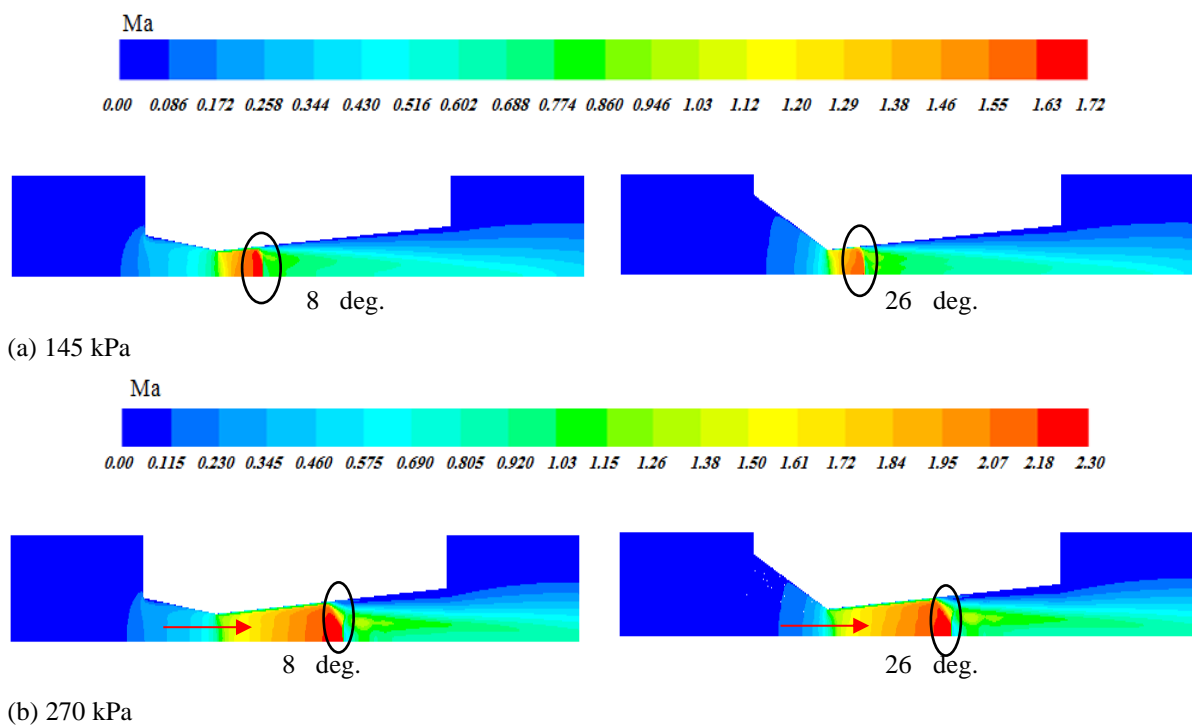


Fig. 17 Mach number contours along convergent-divergent sonic nozzle with different inlet convergence angles with various inlet stagnation pressures.

4. For the cylindrical nozzle, the highest discharge coefficient was observed at $R_c = 1.5 d_{th}$ at a throat diameter of 0.5588 mm, whereas $d_{th} = 3.175$ mm at $R_c = 3d_{th}$.
5. The flow is more uniform with larger throat diameters than with smaller throat diameters. This is due to, reduced boundary layer effects.
6. For the cylindrical nozzle, the velocity gradually increased along the throat region from the beginning to the end of the throat.
7. The cylindrical nozzle reached a normal chock at the end of the throat region due to the effect of the boundary layer on the flow velocity.

CONFLICT OF INTEREST

The authors declared no potential conflicts of interest concerning the research, authorship, and publication of this article.

AUTHORS CONTRIBUTION

Fatma A-M. Kassem: Conceptualization, Methodology, software, Validation, Investigation, resources, Data curation, Writing – original draft, Visualization, and Supervision. **Ali A. Zahran:** Validation, Funding acquisition, Data curation. **Mohamed Adel:** Conceptualization, Data curation, Writing – review & editing, Visualization.

All authors have read and agreed to the published version of the manuscript.

REFERENCES

- Cao, P., Sun, J., Li, C., & Jin, H. (2023). Effect of different parameters on the boundary layer transition position of sonic nozzle. *Measurement*, 222, 113591. <https://doi.org/10.1016/j.measurement.2023.113591>
- Ding, H., Wang, C., & Wang, G. (2016). Approximate solution for discharge coefficient of the sonic nozzle with surface roughness. *Flow Measurement and Instrumentation*, 52, 227-232. <https://doi.org/10.1016/j.flowmeasinst.2016.10.013>
- Ding, H., Wang, C., & Zhao, Y. (2015). Surface roughness effect on flow measurement of real gas in a critical nozzle. *Measurement*, 68, 82-91. <https://doi.org/10.1016/j.measurement.2015.02.038>
- Fluent Inc. *Fluent User's Guide*. Fluent Inc. (2006).
- Hall, I. M. (1962). Transonic flow in two-dimensional and axially-symmetric nozzles. *The Quarterly Journal of Mechanics and Applied Mathematics*, 15(4), 487-508. <https://doi.org/10.1093/qjmam/15.4.487>
- Ishibashi, M. (1999). Discharge coefficient of critical nozzles machined by super-accurate lathes. *Bulletin of NRLM*, 48, 61. ID 10007557560
- Ishibashi, M. (2015). Discharge coefficient equation for critical-flow toroidal-throat venturi nozzles covering the boundary-layer transition regime. *Flow Measurement and Instrumentation*, 44, 107-121. <https://doi.org/10.1016/j.flowmeasinst.2014.11.009>
- Ishibashi, M. (2018). *Effect of a cylindrical throat occasionally produced in a CFVN designed to have a toroidal throat*. National Metrology Institute of Japan, 10th ISFFM Querétaro, Mexico.
- Kassem, F. A., Shaalan, M. R., Hegazy, R. S., & Ibrahim, S. A. (2023). Effect of back pressure and divergence angle on location of normal shock wave. *Journal of Measurement Science & Applications*, 3, 15-31. <https://doi.org/10.21608/jmsa.2023.318495>
- Kliegel, J. R., & Levine, J. N. (1969). Transonic flow in small throat radius of curvature nozzles. *AIAA Journal*, 7(7), 1375-1378. <https://doi.org/10.2514/3.5355>
- Li, C. H., Peng, X. F., & Wang, C. (2010). Influence of diffuser angle on discharge coefficient of sonic nozzles for flow-rate measurements. *Flow Measurement and Instrumentation*, 21(4), 531-537. <https://doi.org/10.1016/j.flowmeasinst.2010.09.003>
- Li, C., & Johnson, A. (2011). Bilateral comparison between NIM's and NIST's gas flow standards. *Mapan*, 26(3), 211-224. <https://doi.org/10.1007/s12647-011-0020-7>
- Li, C., Cao, P., Zhang, H., & Cui, L. (2018). Throat diameter influence on the flow characteristics of a critical Venturi sonic nozzle. *Flow Measurement and Instrumentation*, 60, 105-109. <https://doi.org/10.1016/j.flowmeasinst.2018.02.012>
- Mason, M. L. (1980). *The effect of throat contouring on two-dimensional converging-diverging nozzles at static conditions*. National Aeronautics and Space Administration, Scientific and Technical Information Branch.
- Nakao, S., Asano, H., & Yakuwa, T. (2021). Behaviors of discharge coefficients of small diameter critical nozzles. *Flow Measurement and Instrumentation*, 80, 101994. <https://doi.org/10.1016/j.flowmeasinst.2021.101994>
- Park, K. A., Choi, Y. M., Choi, H. M., Cha, T. S., & Yoon, B. H. (2001). The evaluation of critical pressure ratios of sonic nozzles at low Reynolds numbers. *Flow measurement and Instrumentation*, 12(1), 37-41. [https://doi.org/10.1016/S0955-5986\(00\)00040-6](https://doi.org/10.1016/S0955-5986(00)00040-6)
- Shaalan, M., Kassem, F., & Hagazy, R. (2018). Calibration Nozzle Performance-State of The Art. *The Egyptian International Journal of Engineering Sciences and Technology*, 26(EIJEST, Vol. 26, 2018), 1-13. <https://doi.org/10.21608/eijest.2018.97251>
- Spotts, N. G., Guzik, S., & Gao, X. (2013). *A CFD analysis of compressible flow through convergent-conical nozzles*. 49th AIAA/ASME/SAE/ASEE Joint Propulsion Conference (p. 3734). <https://doi.org/10.2514/6.2013-3734>
- Stratford, B. S. (1964). The calculation of the discharge coefficient of profiled choked nozzles and the optimum profile for absolute air flow measurement. *The Aeronautical Journal*, 68(640), 237-245.

<https://doi.org/10.1017/S0001924000060905>

- Tang, S. P., Purdue Univ Lafayette Ind Project Squid Headquarters. (1969). *Theoretical determination of the discharge coefficients of axisymmetric nozzles under critical flows* (p. 0042). Project SQUID Technical Report. <https://ui.adsabs.harvard.edu/abs/1979rgd..conf..229T>
- Ünsal, B., Rathore, K., & Koç, E. (2016). *Numerical findings on the boundary layer transition of critical-flow venturi nozzles*. *17th International Flow Measurement Conference* (pp. 1-5). https://scholar.google.com/scholar_lookup?title=Numerical%20Findings%20on%20the%20Boundary%20Layer%20Transition%20of%20CriticalFlow%20Venturi%20Nozzles&publication_year=2016&author=B.%20%C3%9Cnsal&author=K.R.%20Rathore&author=E.%20Ko%C3%A7
- Wang, C., Cao, P., Li, C., Ding, H., & Cui, L. (2019). Influence of wall roughness on boundary layer transition position of the sonic nozzles. *Measurement*, *139*, 196-204. <https://doi.org/10.1016/j.measurement.2019.01.091>
- Wang, C., Ding, H., & Zhao, Y. (2014). Influence of wall roughness on discharge coefficient of sonic nozzles. *Flow Measurement and Instrumentation*, *35*, 55-62. <https://doi.org/10.1016/j.flowmeasinst.2013.11.007>
- Weiss, S., Mickan, B., Polansky, J., Oberleithner, K., Bär, M., & Schmelter, S. (2024). Improved prediction of the flow in cylindrical critical flow venturi nozzles using a transitional model. *Flow, Turbulence and Combustion*, 1-27. <https://doi.org/10.1007/s10494-024-00553-3>.
- Zebrowski, B., Jordan, P., & Jaunet, V. (2022). Boundary layer transition in sonic converging-diverging nozzles. *12th International Symposium on Turbulence and Shear Flow Phenomena (TSFP12)*. https://scholar.google.com/scholar?hl=en&as_sdt=0%2C5&q=Boundary+layer+transition+in+sonic+converging-diverging+nozzles.&btnG